Article

Effect of a Tridentate Ligand on the Structure, Electronic Structure, and Reactivity of the Copper(I) Nitrite Complex: Role of the Conserved Three-Histidine Ligand Environment of the Type-2 Copper Site in Copper-Containing Nitrite Reductases

Masato Kujime, Chiemi Izumi, Masaaki Tomura, Masahiko Hada, and Hiroshi Fujii

J. Am. Chem. Soc., **2008**, 130 (19), 6088-6098 • DOI: 10.1021/ja075575b • Publication Date (Web): 16 April 2008

J|A|C|S
ARTICLES

Published on Web 04/16/2008

Effect of a Tridentate Ligand on the Structure, Electronic Structure, and Reactivity of the Copper(I) Nitrite Complex: Role of the Conserved Three-Histidine Ligand Environment of the Type-2 Copper Site in Copper-Containing Nitrite Reductases

Masato Kujime,[†] Chiemi Izumi,[‡] Masaaki Tomura,[†] Masahiko Hada,[‡] and Hiroshi Fujii*,[†]

Institute for Molecular Science and Okazaki Institute for Integrative Bioscience, National Institutes of Natural Sciences, Myodaiji, Okazaki 444-8787, Japan, and Department of Chemistry, Tokyo Metropolitan University, Hachioji, Tokyo 192-0397, Japan

Received July 26, 2007; E-mail: hiro@ims.ac.jp

Abstract: It is postulated that the copper(I) nitrite complex is a key reaction intermediate of copper containing nitrite reductases (Cu-NiRs), which catalyze the reduction of nitrite to nitric oxide (NO) gas in bacterial denitrification. To investigate the structure–function relationship of Cu-NiR, we prepared five new copper(I) nitrite complexes with sterically hindered tris(4-imidazolyl)carbinols [Et-TIC = tris(1-methyl-2-ethyl-4-imidazolyl)carbinol and *i*Pr-TIC = tris(1-methyl-2-isopropyl-4-imidazolyl)carbinol] or tris(1-pyrazolyl)methanes [Me-TPM = tris(3,5-dimethyl-1-pyrazolyl)methane; Et-TPM = tris(3,5-diethyl-1-pyrazolyl)methane; and *i*Pr-TPM = tris(3,5-diisopropyl-1-pyrazolyl)methane]. The X-ray crystal structures of all of these copper(I) nitrite complexes were mononuclear η^1-N-bound nitrite complexes with a distorted tetrahedral geometry. The electronic structures of the complexes were investigated by absorption, magnetic circular dichroism (MCD), NMR, and vibrational spectroscopy. All of these complexes are good functional models of Cu-NiR that form NO and copper(II) acetate complexes well from reactions with acetic acid under anaerobic conditions. A comparison of the reactivity of these complexes, including previously reported (*i*Pr-TACN)Cu(NO_2) [*i*Pr-TACN = 1,4,7-triisopropyl-1,4,7-triazacyclononane], clearly shows the drastic effects of the tridentate ligand on Cu-NiR activity. The copper(I) nitrite complex with the Et-TIC ligand, which is similar to the highly conserved three-histidine ($(His)_3$) ligand environment in the catalytic site of Cu-NiR, had the highest Cu-NiR activity. This result suggests that the $(His)_3$ ligand environment is essential for acceleration of the Cu-NiR reaction. The highest Cu-NiR activity for the Et-TIC complex can be explained by the structural and spectroscopic characterizations and the molecular orbital calculations presented in this paper. Based on these results, the functional role of the $(His)_3$ ligand environment in Cu-NiR is discussed.

Introduction

Denitrification is an important component of the global nitrogen cycle that is responsible for regulating the amount of fixed nitrogen available for plant growth.[1–5] In the denitrification process, some microorganisms couple respiratory adenosine 5′-triphosphate (ATP) synthesis to the reduction of nitrate (NO_3^-) or nitrite (NO_2^-) to dinitrogen gas (N_2) via gaseous nitric oxide (NO) and nitrous oxide (N_2O). The individual reactions of denitrification are catalyzed by distinct reducatases that variously contain Mo, Fe, Cu, or a heme as reaction centers. The reduction of NO_2^- to NO is catalyzed by nitrite reductase, containing either heme cd_1 or copper.

Copper-containing nitrite reductases (Cu-NiRs) have been isolated from bacteria and fungi. The X-ray crystal structures of Cu-NiRs from *Achromobactor cycloclastes*, *Rhodobactor spaerodes*, *Alcaligenes faecalis*, and *Alcaligenes xylosoxidans* show a common reaction center, containing a pair of copper ions, type-1 Cu and type-2 Cu (Figure 1).[6–9] The type-1 Cu site has a $(His)_2$-Cys-Met donor set, which is typical for electron-transfer copper proteins. The type-2 Cu site has three histidine ligands and water as the fourth ligand in the resting state. The type-2 Cu site is thought to be a reaction center where copper-

[†] National Institutes of Natural Sciences.
[‡] Tokyo Metropolitan University.

(1) Kroneck, P. M. H.; Zumft, W. G. In *Denitrification in Soil and Sediment*; Revsbech, N. P., Sorensen, J. , Eds.; Plenum: New York, 1990; pp 1–20.
(2) Adman, E. T.; Turley, S. K. In *Bioinorganic Chemistry of Copper*; Karlin, K. D., Tyeklár, Z., Eds.; Chapman & Hall: New York, 1993; pp 397–405.
(3) Averill, B. A. *Chem. Rev.* **1996**, *96*, 2951–2964.
(4) Suzuki, S.; Kataoka, K.; Yamaguchi, K.; Inoue, T.; Kai, Y. *Coord. Chem. Rev.* **1999**, *190–192*, 245–265.
(5) Wasser, I. M.; de Vries, S.; Moénne-Loccoz, P.; Schröder, I.; Karlin, K. D. *Chem. Rev.* **2002**, *102*, 1201–1234.
(6) (a) Godden, J. W.; Turley, S.; Teller, D. C.; Adman, E. T.; Liu, M. Y.; Payne, W. J.; LeGall, J. W. *Science* **1991**, *253*, 438–442. (b) Adman, E. T.; Godden, J. W.; Turley, S. *J. Biol. Chem.* **1995**, *270*, 27458–27474.
(7) (a) Jacobson, F.; Guo, H.; Olesen, K.; Okvist, M.; Neutze, R.; Sjölin, L. *Acta Crystallogr., Sect. D: Biol. Crystallogr.* **2005**, 1190–1198. (b) Jacobson, F.; Pistorius, A.; Farkas, D.; De Grip, W.; Hansson, O.; Sjölin, L.; Neutze, R. *J. Biol. Chem.* **2007**, *282*, 6347–6355.

 10.1021/ja075575b CCC: $40.75

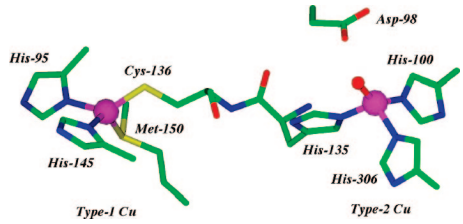

Figure 1. 3D view of the active site structure of nitrite reducatase (NiR) from *Alcaligenes faecalis*, created from the coordinates obtained from PDB file 1AS7.

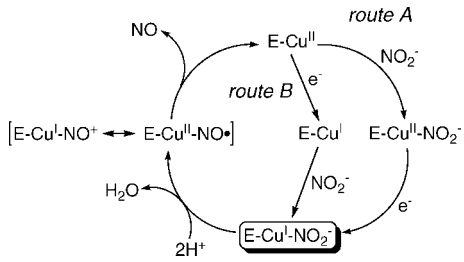

Figure 2. Proposed reaction mechanism for nitrite reduction by Cu-NiR.

bound nitrite is reduced to NO with electrons transferred from the type-1 Cu site via a Cys−His bridge and protons donated via conserved amino acid residues, for example, Asp-98 and His-255 in *Alcaligenes faecalis* (Figure 1).[6a,10–12] In the nitrite reduction by Cu-NiRs, the nitrite adduct of a reduced type-2 Cu site, namely, the copper(I) nitrite complex, and the NO adduct of an oxidized type-2 Cu site, namely, the copper(II) NO complex, have been proposed as key reaction intermediates (Figure 2).[13,14] However, these intermediates have not been detected in the catalytic cycle of Cu-NiR, probably because of their high reactivity. The characterization of these intermediates is thought to be a key to understanding the reaction mechanism of Cu-NiR.

As a result, considerable attention has been directed to the structure and reactivity of the copper(I) nitrite complex. While various copper(II) nitrite complexes have been prepared from various N-donor ligands to mimic the $(His)_3$ environment of the type-2 Cu site,[15–25] only a few copper(I) nitrite complexes have been isolated.[25–28] Halfen et al. reported the first and only structurally well-characterized model complex, (*i*Pr-TACN)-Cu(NO_2) (*i*Pr-TACN = 1,4,7-triisopropyl-1,4,7-triazacyclononane), which forms NO by reaction with 2 equiv of acetic acid.[27,28] These model studies revealed that nitrite binds with O-coordination to the copper(II) ion as well as with N-coordination to the copper(I) ion. Recently, we succeeded in the first detection of the nitrous acid intermediate (Cu−NO_2H) in a nitrite reduction by rapid mixing of (*i*-Pr-TACN)Cu(NO_2) with trifluoroacetic acid at low temperature.[29] In contrast, nitrite adducts of the type-2 Cu site were prepared by soaking nitrite into Cu-NiR crystals; their X-ray crystal structures showed O-coordination of nitrite to the oxidized type-2 Cu site.[6b,7b,8b,c,9c,10b,30] A recent X-ray crystal study of the NO adduct of the reduced type-2 Cu site reported a unique side-on NO coordination and a reaction mechanism, in which the nitrite binds to the oxidized type-2 Cu site followed by reduction (see route A in Figure 2).[8c] While the reaction of Cu-NiR has been studied from both enzymatic and synthetic model systems, the structure, reactivity, and reaction mechanism of the copper(I) nitrite complex remains controversial.

In this paper, we show the preparation of five new copper(I) nitrite complexes with sterically hindered tris(4-imidazolyl)-carbinol (TIC)[31] or tris(1-pyrazolyl)methane (TPM) ligands to mimic the $(His)_3$ environment in the type-2 Cu site in Cu-NiR (Figure 3): (Et-TIC)Cu(NO_2) (Et-TIC = tris(1-methyl-2-ethyl-4-imidazolyl)carbinol), (*i*Pr-TIC)Cu(NO_2) (*i*Pr-TIC = tris(1-methyl-2-isopropyl-4-imidazolyl)carbinol), (Me-TPM)Cu(NO_2) (Me-TPM = tris(3,5-dimethyl-1-pyrazolyl)methane), (Et-TPM)Cu(NO_2) (Et-TPM = tris(3,5-diethyl-1-pyrazolyl)methane), and (*i*Pr-TPM)Cu(NO_2) (*i*Pr-TPM = tris(3,5-diisopropyl-1-pyrazolyl)methane). These complexes were characterized using X-ray crystallography and various spectroscopic methods. All of these copper(I) nitrite complexes are good functional models of Cu-NiR that form NO and copper(II) acetate complexes well from reactions with acetic acid under anaerobic conditions.

(8) (a) Murphy, M. E. P.; Turley, S.; Kukimoto, M.; Nishiyama, M.; Horinouchi, S.; Sasaki, H.; Tanoruki, M.; Adman, E. T. *Biochemistry* **1995**, *34*, 12107–12117. (b) Murphy, M. E. P.; Turley, S.; Adman, E. T. *J. Biol. Chem.* **1997**, *272*, 28455–28460. (c) Tocheva, E. I.; Rosell, F. I.; Mauk, A. G.; Murphy, M. E. P. *Science* **2004**, *304*, 867–870.
(9) (a) Dodd, F. E.; Hasnain, S. S.; Abraham, Z. H. L.; Eady, R. R.; Smith, B. E. *Acta Crystallogr. D* **1997**, *53*, 406–418. (b) Dodd, F. E.; Van Beeumen, J.; Eady, R. R.; Hasnain, S. S. *J. Mol. Biol.* **1998**, *282*, 369–382. (c) Antonyuk, S. V.; Strange, R. W.; Sawers, G.; Eady, R. R.; Hasnain, S. *Proc. Natl. Acad. Sci. U.S.A.* **2005**, *102*, 12041–12046.
(10) (a) Boulanger, M. J.; Kukimoto, M.; Nishiyama, M.; Horinouchi, S.; Murphy, M. E. P. *J. Biol. Chem.* **2000**, *275*, 23957–23964. (b) Boulanger, M. J.; Murphy, M. E. P. *Biochemistry* **2001**, *40*, 9132–9141.
(11) Kataoka, K.; Rurusawa, K.; Takagi, H.; Yamaguchi, K.; Suzuki, S. *J. Biochem.* **2000**, *197*, 345–350.
(12) Zhao, Y.; Lukoyanov, D. A.; Toropov, Y. V.; Wu, K.; Sharleigh, J. P.; Scholes, C. P. *Biochemistry* **2002**, *41*, 7464–7474.
(13) Strange, R. W.; Murphy, L. M.; Dodd, F. E.; Abraham, Z. H.; Eady, R. R.; Smith, B. E.; Hasnain, S. S. *J. Mol. Biol.* **1999**, *287*, 1001–1009.
(14) (a) Weeg-Aerssens, E.; Tiedje, J. M.; Averill, B. A. *J. Am. Chem. Soc.* **1988**, *110*, 6851–6856. (b) Hulse, C. L.; Averill, B. A.; Tiedje, J. M. *J. Am. Chem. Soc.* **1989**, *111*, 2322–2323. (c) Jackson, M. A.; Tiedje, J. M.; Averill, B. A. *FEBS Lett.* **1991**, *291*, 41–44. (d) Ye, R. W.; Toro-Suarez, I.; Tiedje, J. M.; Averill, B. A. *J. Biol. Chem.* **1991**, *266*, 12848–12851.
(15) Tolman, W. B. *Inorg. Chem.* **1991**, *30*, 4877–4880.
(16) Komeda, N.; Nagao, H.; Adachi, G.; Suzuki, M.; Uehara, A.; Tanaka, K. *Chem. Lett.* **1993**, 1521–1524.
(17) Jiang, F.; Conry, R. R.; Bubacco, L.; Tyeklár, Z.; Jacobson, R. R.; Kalin, K. D.; Peisach, J. *J. Am. Chem. Soc.* **1993**, *115*, 2093–2102.
(18) Ruggiero, C. E.; Carrier, S. M.; Tolman, W. B. *Angew. Chem., Int. Ed. Engl.* **1994**, *33*, 895–897.
(19) Komeda, N.; Nagao, H.; Kushi, Y.; Adachi, G.; Suzuki, M.; Uehara, A.; Tanaka, K. *Bull. Chem. Soc. Jpn.* **1995**, *68*, 581–589.
(20) Stibrany, R. T.; Potenza, J. A.; Schugar, H. J. *Inorg. Chim. Acta* **1996**, *243*, 33–37.
(21) Casella, L.; Carugo, O.; Gullotti, M.; Doldi, S.; Frassoni, M. *Inorg. Chem.* **1996**, *35*, 1101–1113.
(22) Schneider, J. L.; Carrier, S. M.; Ruggiero, C. E.; Young, V. G., Jr.; Tolman, W. B. *J. Am. Chem. Soc.* **1998**, *120*, 11408–11418.
(23) Monzani, E.; Koolhaas, G. J. A. A.; Spandre, A.; Leggieri, E.; Casella, L.; Gullotti, M.; Nardin, G.; Randaccio, L.; Fontani, M.; Zanello, P.; Reedijk, J. *J. Biol. Inorg. Chem.* **2000**, *5*, 251–261.
(24) Scarpellini, M.; Neves, A.; Castellano, E. E.; de Almeida Neves, E. F.; Franco, D. W. *Polyhedron* **2004**, *23*, 511–518.
(25) Yokoyama, H.; Yamaguchi, K.; Sugimoto, M.; Suzuki, S. *Eur. J. Inorg. Chem.* **2005**, 1435–1441.
(26) Halfen, J. A.; Mahapatra, S.; Olmstead, M. M.; Tolman, W. B. *J. Am. Chem. Soc.* **1994**, *116*, 2173–2174.
(27) Halfen, J. A.; Tolman, W. B. *J. Am. Chem. Soc.* **1994**, *116*, 5475–5476.
(28) Halfen, J. A.; Mahapatra, S.; Wilkinson, E. C.; Gengenbach, A. J.; Young, V. G., Jr.; Que, L., Jr.; Tolman, W. B. *J. Am. Chem. Soc.* **1996**, *118*, 763–776.
(29) Kujime, M.; Fujii, H. *Angew. Chem., Int. Ed.* **2006**, *45*, 1089–1092.
(30) Tocheva, E. I.; Rosell, F. I.; Mauk, A. G.; Murphy, M. E. *Biochemistry* **2007**, *46*, 12366–12374.
(31) Kujime, M.; Fujii, H. *Tetrahedron Lett.* **2005**, *46*, 2809–2812.

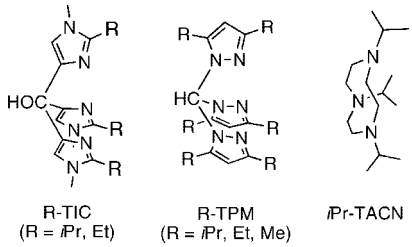

Figure 3. Structures of N donor tridentate ligands used in this study.

Comparison of the reactivity of these complexes with that of (*i*Pr-TACN)Cu(NO_2) clearly showed that the Cu-NiR activity is drastically changed by the steric and electronic effects of the tridentate ligand; Et-TIC had the highest activity of the complexes. Structural and spectroscopic characterization, as well as molecular orbital (MO) calculations, indicate how the tridentate ligand modulates the Cu-NiR activity of the copper(I) nitrite complex. In the last part of this paper, we discuss the functional role of the $(His)_3$ environment in the type-2 Cu site of Cu-NiR on the basis of the present model study.

Results

Crystal Structure. Copper(I) nitrite complexes of TIC and TPM ligands, (*i*Pr-TIC)Cu(NO_2), (Et-TIC)Cu(NO_2), (*i*Pr-TPM)Cu(NO_2), (Et-TPM)Cu(NO_2), and (Me-TPM)Cu(NO_2), were prepared from the reactions of the corresponding copper(I) acetonitrile complexes with $[(Ph_3P)_2N]NO_2$ in either an acetone or acetone−CH_2Cl_2 mixture. This method was previously attempted for the synthesis of copper(I) nitrite complexes.[25,28] However, for (*i*Pr-TACN)Cu(NO_2), this resulted in a decomposition of the nitrite complex with NO formation.[28] Successful preparations for the TIC and TMP complexes by this method may have been due to the low solubility of these copper(I) nitrite complexes in acetone, leading to precipitation of the products from the reaction mixtures. Recrystallization of the nitrite complexes precipitated out from the reaction mixtures gave single crystals suitable for X-ray crystallography.

The crystal structures of (*i*Pr-TIC)Cu(NO_2), (Et-TIC)Cu(NO_2), (*i*Pr-TPM)Cu(NO_2), (Et-TPM)Cu(NO_2), and (Me-TPM)Cu(NO_2) are shown in Figure 4. Selected bond lengths and angles of these complexes are listed in Table 1 with those of (*i*Pr-TACN)Cu(NO_2) for comparison.[27] As shown in Figure 4, tridentate ligands bind to copper ions in a κ^3-manner and the nitrite ions are bound to copper in a η^1-N coordination manner in all complexes. The interligand bond angles (83 ∼ 92°) between the N atoms of the tridentate ligand, N−Cu−N_L, are smaller than those (116 ∼ 138°) between the N atom of the tridentate ligand and the N atom of the copper-bound nitrite, N−Cu−$N_{nitrite}$. The coordination geometries of the copper(I) ions in all copper(I) nitrite complexes are described as distorted tetrahedral symmetries. The terminal methyl groups of isopropyl substituents in (*i*Pr-TIC)Cu(NO_2) are directed to the metal center possibly due to the steric influence of the adjacent N-methyl groups. The same behavior has been reported for other copper(I) complexes of the *i*Pr-TIC ligand, [(*i*Pr-TIC)Cu(CH_3CN)]ClO_4 and [(*i*Pr-TIC)Cu(CO)]ClO_4.[31,32] In contrast, the terminal methyl groups of (*i*Pr-TPM)Cu(NO_2) and (*i*Pr-TACN)Cu(NO_2) are directed outward. Therefore, in the solid state, the isopropyl substituent in (*i*Pr-TIC)Cu(NO_2) functions as a *tert*-butyl group

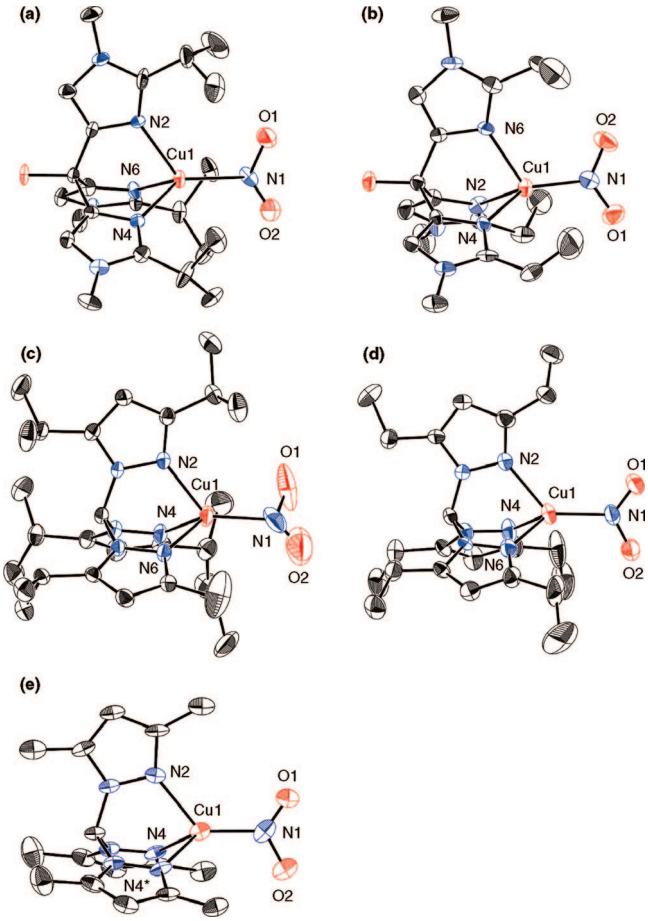

Figure 4. ORTEP drawing of (a) (*i*Pr-TIC)Cu(NO_2), (b) (Et-TIC)Cu(NO_2), (c) (*i*Pr-TPM)Cu(NO_2), (d) (Et-TPM)Cu(NO_2), and (e) (Me-TPM)Cu(NO_2) showing all nonhydrogen atoms with thermal ellipsoids at the 50% probability level.

and the steric effect of the isopropyl substituent in the *i*Pr-TIC ligand is more significant than that in the *i*Pr-TPM and *i*Pr-TACN ligands.

The structural parameters of copper(I) nitrite complexes are changed by the tridentate ligand. As shown in Table 1, the Cu−$N_{nitrite}$ bond length of (L)Cu(NO_2) is increased in the order of Me-TPM (1.883 Å) ≈ Et-TIC (1.889 Å) < *i*Pr-TACN (1.903 Å) < Et-TPM (1.952 Å) < *i*Pr-TPM (2.010 Å) < *i*Pr-TIC (2.030 Å). For both the TIC and TPM ligands, the increasing steric bulk of the substituents correlates to the longer Cu−$N_{nitrite}$ bond. The steric interaction between the copper-bound nitrite and the substituent may modulate the Cu−$N_{nitrite}$ bond length. The O−N−O bond angles (116.6 ∼ 122.1°) of the copper-bound nitrites are comparable to the angles for monodentate N-bound nitrite complexes.[33] The average of three Cu−N_L bond lengths of (L)Cu(NO_2) increases in the order of Et-TIC (2.063 Å) < Me-TPM (2.075 Å) < Et-TPM (2.091 Å) ≈ *i*Pr-TPM (2.093 Å) < *i*Pr-TIC (2.129 Å) < *i*Pr-TACN (2.163 Å). As for the Cu−$N_{nitrite}$ bond length, the average Cu−N_L bond length increases with an increase in the steric effect of the substituent. The steric interaction between the copper-bound nitrite and the substituent also may modulate the Cu−N_L bond length. The average Cu−N_L bond lengths of copper(I) nitrite complexes with imino-type ligands (TIC and TPM) are much shorter than those

(32) Kujime, M.; Kurahashi, T.; Tomura, M.; Fujii, H. *Inorg. Chem.* **2007**, *46*, 541–551.

(33) Hitchman, M. A.; Rowbottom, G. L. *Coord. Chem. Rev.* **1982**, *42*, 55–132.

Table 1. Selected Bond Distances (Å) and Angles (deg) for Copper(I) Nitrite Complexes and the Type-2 Cu Site in Cu-NiR

	$Cu-N_{nitrite}$	N−O	$Cu-N_L$	O−N−O	$N_L-Cu-N_{nitrite}$	N_L-Cu-N_L	ref
(*i*Pr-TIC)Cu(NO_2)	2.030 (7)	1.256 (10)	2.180 (7)	122.1 (8)	122.4 (3)	87.8 (3)	this work
		1.15 (1)	2.108 (7)		128.4 (3)	89.8 (3)	
			2.098 (6)		127.8 (3)	88.0 (3)	
(Et-TIC)Cu(NO_2)	1.889 (6)	1.237 (7)	2.068 (6)	116.7 (7)	116.3 (2)	88.0 (2)	this work
		1.208 (6)	2.032 (5)		141.9 (2)	92.1 (2)	
			2.088 (5)		119.4 (2)	86.2 (2)	
(*i*Pr-TPM)Cu(NO_2)	2.010 (4)	1.316 (8)	2.087 (3)	118.3 (9)	130.6 (1)	86.1 (1)	this work
		1.136 (10)	2.094 (3)	119.7 (9)[a]	126.9 (1)	86.5 (1)	
		1.341 (9)[a]	2.099 (3)		125.5 (2)	87.00 (10)	
		1.078 (10)[a]					
(Et-TPM)Cu(NO_2)	1.952 (7)	1.25 (1)	2.137 (7)	117.0 (8)	130.2 (3)	86.5 (3)	this work
		1.22 (1)	2.080 (7)		125.6 (3)	85.3 (3)	
			2.056 (6)		127.1 (3)	88.2 (3)	
(Me-TPM)Cu(NO_2)	1.883 (6)	1.278 (7)	2.124 (5)	117.4 (5)	128.4 (2)	86.2 (2)	this work
		1.176 (7)	2.051 (3)		126.7 (1)	87.6 (1)	
			2.051 (3)		126.7 (1)	87.6 (2)	
(*i*Pr-TACN)Cu(NO_2)	1.903 (4)	1.253 (5)	2.133 (3)	116.6 (4)	123.9 (1)	86.5 (1)	27
		1.238 (5)	2.157 (3)		138.4 (1)	83.5 (1)	
			2.199 (4)		124.0 (1)	83.2 (1)	
reduced Cu-NiR			1.94 (4)			108 (1)	8b
			2.01 (8)			106 (4)	
			2.06 (2)			125 (3)	

[a] O atoms in the copper-bound nitrite were found to be disordered (see Experimental Section).

Table 2. Summary of Selected Spectroscopic Data for Copper(I) Nitrite Complexes

complex	UV–vis λ_{max}/nm (ϵ/M^{-1} cm^{-1}) in CH_2Cl_2	FT-IR cm^{-1} (KBr or CsI pellet)[a]	CV $E_{1/2}$/volt vs SCE[b]	^{15}N NMR $\delta(^{15}NO_2)$/ ppm from $^{15}NO_3^-$
(*i*Pr-TIC)Cu(NO_2)	290 (3900)	1320 (1296), 1253 (1235), 831 (824), 402 (393)	0.15 (0.33)	153.6
(Et-TIC)Cu(NO_2)	289 (3600)	1310 (1286), 1248 (1221), 823 (814), 401 (385)	0.16 (0.28)	167.4
(iPr-TPM)Cu(NO_2)	263 (6700), 296 (sh, 5000)	1311 (1289), 1282 (1263), 814 (808), 392 (379)	0.27 (0.35)	148.3
(Et-TPM)Cu(NO_2)	263 (6200), 295 (sh, 4800)	1310 (1287), 1283 (1261), 813 (806), 402 (392)	0.26 (0.35)	147.5
(Me-TPM)Cu(NO_2)	263 (5900), 293 (sh, 4700)	1314 (1289), 1280 (1258), 822 (814), 411 (401)	0.25 (0.27)	147.2
(*i*Pr-TACN)Cu(NO_2)	308 (3800)[b]	1306, 1268 (1247), 809 (803), 398, 390 (383)	0.10 (0.25)	145.9

[a] Wavenumbers for ($^{15}NO_2$)-labeled complexes are shown in parenthesis. [b] In CH_2Cl_2 containing 0.1 M (n-Bu_4N)(ClO_4) as electrolyte, scan rate: 50 mV s^{-1}. The numbers in parentheses are ΔE_p (E_{pa}–E_{pc}) values.

with amino-type ligands (TACN). The same result has been observed for the copper(I) acetonitrile and CO complexes of these tridentate ligands.[31,32] If the significant steric effect of the isopropyl substituent in *i*Pr-TIC is taken into account, the TIC ligand would have a stronger interaction with the copper(I) ion than the two other ligands, TPM and TACN.

Spectroscopic Characterization. The structures of copper(I) nitrite complexes in solution were further characterized by ^1H and ^{15}N NMR spectroscopy. The ^1H NMR spectra of (Et-TIC)Cu(NO_2) and (*i*Pr-TIC)Cu(NO_2) in CD_2Cl_2 showed only one set of sharp ^1H NMR signals for three imidazole rings and substituents, together with one bridgehead C−OH signal. This indicates that three imidazole rings in (Et-TIC)Cu(NO_2) and (*i*Pr-TIC)Cu(NO_2) are equivalent within the NMR time scale in solution because of rapid fluctuation. Similar results were obtained for (Me-TPM)Cu(NO_2), (Et-TPM)Cu(NO_2), and (*i*Pr-TPM)Cu(NO_2) in CD_2Cl_2. We also measured the ^{15}N NMR spectra of the copper-bound nitrites of copper(I) nitrite complexes with ^{15}N-labeled samples (Table 2). The ^{15}N NMR signals showed drastic upfield shifts from the free nitrite ion in the order of TIC < TPM < TACN, indicating that the nitrite ions are bound to copper(I) even in solution.

UV−vis absorption spectra of the copper(I) nitrite complexes are shown in Figure 5a and Figure S1 of the Supporting Information. Absorption maxima are summarized in Table 2. The spectral feature and the absorption maxima are hardly changed by the steric effect of the substituents of the TIC and TPM ligands. A strong absorption observed at 308 nm for (*i*Pr-TACN)Cu(NO_2) has been assigned as a metal-to-ligand charge transfer (MLCT) band.[28] (Et-TIC)Cu(NO_2) and (*i*Pr-TIC)-Cu(NO_2) also exhibit strong absorption at 290 nm, while (Me-TPM)Cu(NO_2), (Et-TPM)Cu(NO_2), and (*i*Pr-TPM)Cu(NO_2) show strong absorption at 263 nm and shoulder absorption near

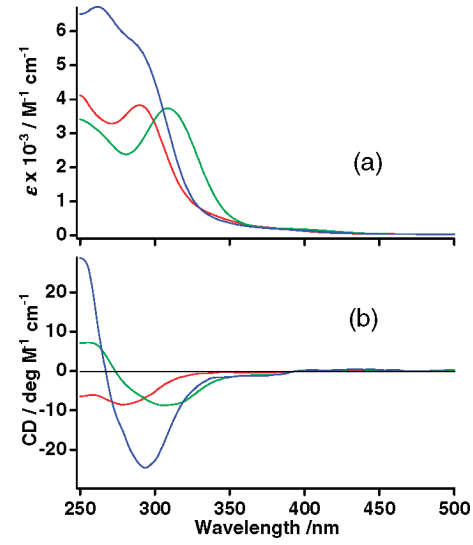

Figure 5. Electronic absorption spectra (a) and MCD spectra with 1.0 T (b) of copper(I) nitrite complexes (0.25 mM) in CH_2Cl_2 at room temperature. Red line, (*i*Pr-TIC)Cu(NO_2); blue line, (*i*Pr-TPM)Cu(NO_2); and green line, (*i*Pr-TACN)Cu(NO_2).

295 nm. To further investigate absorption in the UV region for TIC and TPM complexes, we examined the magnetic circular dichroism (MCD) spectra of these copper(I) nitrite complexes, as shown in Figure 5b and Figure S1 of the Supporting Information. The transition corresponding to the absorption at 308 nm for (*i*Pr-TACN)Cu(NO_2) shows a negative MCD peak. Similarly, the transitions corresponding to the absorptions at 290 nm for (*i*Pr-TIC)Cu(NO_2) and (Et-TIC)Cu(NO_2) exhibited negative MCD peaks. The transitions corresponding to the shoulder peaks near 295 nm for (Me-TPM)Cu(NO_2), (Et-TPM)Cu(NO_2), and (*i*Pr-TPM)Cu(NO_2) showed negative MCD peaks, but the transitions at 263 nm did not. Therefore, absorptions at 290 nm for the TIC complexes and absorptions near 295 nm for the TPM complexes can be assigned to the MLCT bands. The MLCT band shifts to lower energy in the order of TIC < TPM < TACN, which is identical to the order of the ^{15}N NMR shift of the copper-bound nitrite.

Cyclic voltammetry of copper(I) nitrite complexes was carried out, and the results are summarized in Figure S2 of the Supporting Information and Table 2. All of the copper(I) nitrite complexes in CH_2Cl_2 containing 0.1 M (*n*-Bu_4N)(ClO_4) exhibited quasi-reversible one-electron redox peaks, which we assign to Cu(I)/Cu(II) redox processes. As shown in Table 2, the redox potential, $E_{1/2}$, of the copper(I) nitrite complex is sensitive to the nature of the tridentate ligand, but not sensitive to the steric effect of the substituent of the tridentate ligand. The $E_{1/2}$ value increases in the order of TACN < TIC < TPM. Since the Cu(I)/Cu(II) redox potential was shown to correlate with the stability constant of its copper(II) complex,[34] the order of the redox potentials of copper(I) nitrite complexes would also reflect the order of the stabilities of the copper(II) nitrite complexes, as well as the electron densities of the copper(I) ions. While the copper(I) nitrite complexes have the distorted tetrahedral structures as shown in previous and present studies, the copper(II) nitrite complexes have distorted square pyramidal or trigonal bipyramidal structures.[15,18,21,25,26] Therefore, the TACN ligand may stabilize the structure of the copper(II) state more than the TIC and TPM ligands. Alternatively, the ligand structure and/or electronic effect of the TIC and TPM ligands may stabilize the copper(I) state more than those of the TACN ligand.

Infrared (IR) spectra of copper(I) nitrite complexes exhibited bands sensitive to $^{15}NO_2^-$ substitution (Figure S3 of the Supporting Information and Table 2). The ^{15}N sensitive bands at 1306 and 1268 cm^{-1} for (*i*Pr-TACN)Cu(NO_2) were previously assigned to the nitrite asymmetric (ν_{as}) and symmetric (ν_s) stretches, respectively.[28] Similar bands were observed for the TIC and TPM complexes. The bands for ν_{as} and ν_s stretches of the copper-bound nitrites in (Et-TIC)Cu(NO_2) and (*i*Pr-TIC)Cu(NO_2) were detected at 1312 and 1248 cm^{-1} and at 1320 and 1262 cm^{-1}, respectively. Similarly, the bands for ν_{as} and ν_s stretches of the copper-bound nitrites in TPM complexes were observed at around 1310 and 1280 cm^{-1}, respectively. Other ^{15}N sensitive bands for the copper(I) nitrite complexes were observed at around 800 cm^{-1}, which were assigned as a scissor-mode (δ) from comparison of these frequencies and isotope shifts (6 $\sim$ 9 cm^{-1}) with those of other transition metal η^1-NO_2^- complexes reported previously.[33] To assign the copper-nitrite vibrational frequencies, we further measured far-IR spectra of copper(I) nitrite complexes between 150 and 600 cm^{-1} (Figure S4 of the Supporting Information and Table 2). For all complexes prepared in this study, we found bands sensitive to $^{15}NO_2^-$ substitution at around 400 cm^{-1}. With ^{15}N substitution of the copper-bound nitrite, the bands around 400 cm^{-1} were shifted to a lower frequency by about 10 cm^{-1}. In comparing these frequencies and isotope shifts with those of other transition metal η^1-NO_2^- complexes reported previously,[33] these bands were assigned to Cu$-$N$_{nitrite}$ stretches (ν_{Cu-N}). The ν_{Cu-N} bands for copper(I) nitrite complexes indicate that the Cu$-$N$_{nitrite}$ bond becomes stronger with a decrease in the steric effect of the substitutent, *i*Pr < Et < Me, and, for the same substituent, it is in the order of TPM < TACN < TIC.

Reaction with Acetic Acid. Previous studies have reported that copper(I) nitrite complexes react with 2 equiv of acetic acid to yield copper(II) acetate complexes and NO under anaerobic conditions.[23,25,28] To investigate the validity of the copper(I) nitrite complexes with TIC and TMP ligands as a functional Cu-NiR model, we examined the reactions with acetic acid. Figures 6 and S5 of the Supporting Information show UV–vis absorption spectral changes for the reactions of copper(I) nitrite complexes with 5 equiv of acetic acid in CH_2Cl_2 under anaerobic conditions. As previously reported,[28] the absorption spectrum of (*i*Pr-TACN)Cu(NO_2) is changed to that of (*i*Pr-TACN)-Cu(CH_3CO_2)$_2$ with clear isosbestic points upon addition of acetic acid (Figure 6c). Similarly, the absorption spectra of (*i*Pr-TIC)Cu(NO_2) and (*i*Pr-TPM)Cu(NO_2) change to new ones with weak absorptions around 700 nm with isosbestic points under anaerobic conditions (Figure 6a and 6b). The absorption spectra of the reaction products for the TIC and TPM complexes are close to that of (*i*Pr-TACN)Cu(CH_3CO_2)$_2$, suggesting the formation of copper(II) complexes. Moreover, electron paramagnetic resonance (EPR) spectral measurements clearly showed the formation of copper(II) complexes from copper(I) nitrite complexes in these reactions (see insets in Figure 6 and S5 of the Supporting Information). The ESI-MS analysis of the reaction solutions for the TIC and TPM complexes exhibited major mono cation peaks corresponding to copper(II) mono acetate complexes. To further identify the reaction products for the TIC and TPM complexes, we tried to isolate these complexes as solids. The blue-green complexes isolated from the reaction solutions of (Et-TIC)Cu(NO_2) and (*i*Pr-TIC)Cu(NO_2) were identified as (Et-TIC)Cu(CH_3CO_2)$_2$ and (*i*Pr-TIC)Cu(CH_3CO_2)$_2$, respectively, on the basis of a comparison of their UV–vis, EPR, and IR spectra to those of independently synthesized complexes as well as their elemental analysis (Table 3). In contrast, the blue complexes isolated from the reaction solutions of the TPM complexes were identified as copper(II) acetate, Cu(CH_3CO_2)$_2$, because of instabilities in the copper(II) acetate complexes of the TPM ligands in the solid state, which led to decomposition of the products during the isolation processes. Titration experiments of copper(I) nitrite complexes with acetic acid clearly showed that 2 equiv of acetic acid were consumed in these reactions (see Figure S6 of the Supporting Information). To confirm NO generation from these reactions, the generating NO gas was trapped using an iron(II) octaethylporphyrin (OEP) complex that has high affinity for NO.[35] EPR measurements of the trapped solutions at room temperature showed a strong three-line EPR signal due to a hyperfine coupling (A = 1.53 mT) with the iron-bound ^{14}NO at g = 2.05, which is typical for iron(II) porphyrin NO complexes (see Figure S7 of the Sup-

(34) Ambundo, E.; Deydier, M.-V.; Grall, A. J.; Aguera-Vega, N.; Dressel, L. T.; Cooper, T. H.; Heeg, M. J.; Ochrymowycz, L. A.; Rorabacher, D. B. *Inorg. Chem.* **1999**, *38*, 4233–4242.

(35) (a) Adachi, H.; Sonoki, H.; Hoshino, M.; Wakasa, M.; Hayashi, H.; Miyazaki, Y. *J. Phys. Chem. A* **2001**, *105*, 392–398. (b) Tsai, A.-L. *FEBS Lett.* **1994**, *341*, 141–145.

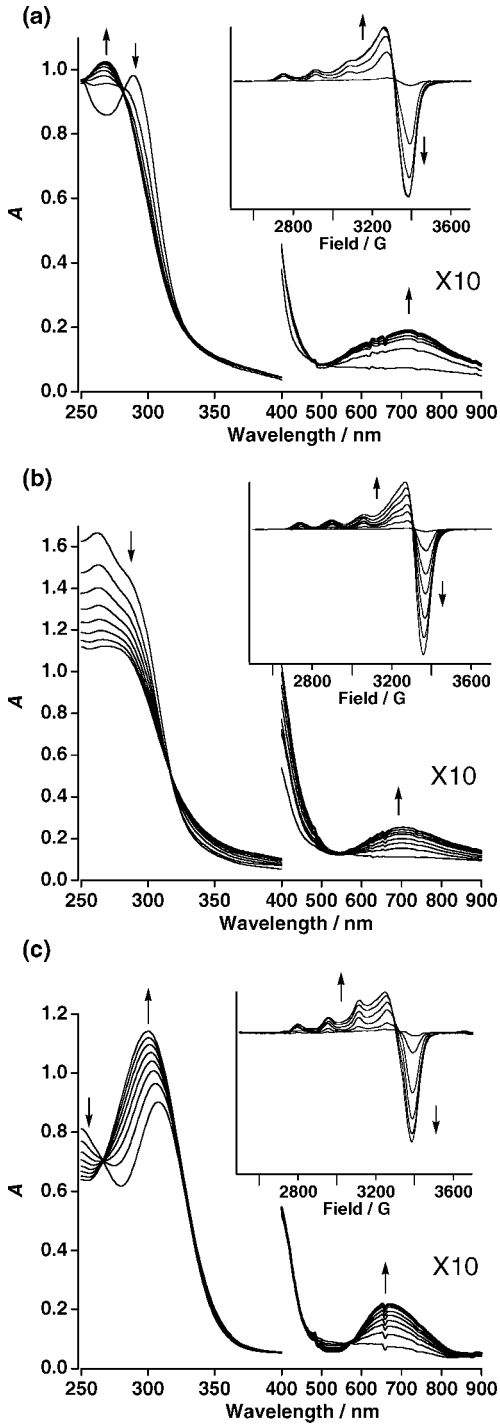

Figure 6. Changes in UV–vis and EPR (inset) spectra for the reaction of 0.25 mM (a) (*i*Pr-TIC)Cu(NO_2) (UV–vis: 5 min interval, EPR: 0, 5, 10, 20, and 30 min), (b) (*i*Pr-TPM)Cu(NO_2) (UV–vis: 30 min interval, EPR: 0, 10, 20, 40, 60, 120, and 180 min), and (c) (*i*Pr-TACN)Cu(NO_2) (UV–vis: 15 min interval, EPR: 0, 2, 10, 20, 30, and 40 min) with 5 equiv of acetic acid (1.25 mM) in CH_2Cl_2 at room temperature.

porting Information).[36] From the intensities of the EPR signals, it was estimated that about 70% of NO was trapped for all complexes. These results indicate that the copper(I) nitrite complexes with TIC and TPM ligands are good functional Cu-NiR models that produce copper(II) acetate complexes and NO with 2 equiv of acetic acid under anaerobic conditions.

(36) Wayland, B. B.; Olson, L. W. *J. Am. Chem. Soc.* **1974**, *96*, 6037–6041.

Cu-NiR Activity. To compare the Cu-NiR activity of these copper(I) nitrite complexes, we estimated the reaction rates with acetic acid in CH_2Cl_2 at 293 K. Under an excess of acetic acid, the time courses of the absorption changes for the reactions of all of these copper(I) nitrite complexes were fit well with a single exponential function (Figure S8 and Table S3 of the Supporting Information). The apparent reaction rate constants under excess acetic acid did not depend on the concentration of the copper(I) nitrite complexes (Figure S9 of the Supporting Information). These results clearly show that the reactions are first-order with respect to the copper complexes. Figure 7 shows plots of pseudo first-order rate constants, k_{obs}, against the concentration of acetic acid. The plots provide curved lines rather than linear ones. Since 2 equiv of acetic acid was reacted, we attempted to simulate the dependence of k_{obs} with the equation derived from the second-order reaction for acetic acid (Scheme 1 and eq1).

$$k_{obs} = k[CH_3COOH]^2 \quad (1)$$

However, the dependence of the rate constants k_{obs} could not be simulated well with eq1, suggesting a stepwise proton transfer mechanism as proposed in a previous stopped-flow experiment.[29] Based on the reaction mechanism shown in Scheme 2, eq2 was derived with a steady-state approximation for the intermediate, (L)CuNO_2H.

$$k_{obs} = \frac{k_1[CH_3COOH]^2}{(k_{-1}/k_2) + [CH_3COOH]} \quad (2)$$

According to this equation, it can be expected that k_{obs} would be proportional to the concentration of acetic acid if the rate of the second protonation step, k_2, is much larger than that of the deprotonation step, k_{-1}, ($k_2 >> k_{-1}$: $k_{-1}/k_2 \approx 0$) while the dependence of k_{obs} would be curved when k_{-1}/k_2 is comparable to the concentration of acetic acid. As shown in Figure 7, the dependence of k_{obs} on the concentration of acetic acid is fit well with eq2 and the estimated k_1 and k_{-1}/k_2 values are summarized in Table 4. The k_1 and k_{-1}/k_2 values are changed by the tridentate ligand. In particular, the extremely high reactivity of (Et-TIC)Cu(NO_2) is worth noting. The k_1 value is increased in the order of *i*Pr-TPM < Et-TPM < Me-TPM < *i*Pr-TIC < *i*Pr-TACN << Et-TIC, and the k_{-1}/k_2 value is increased in the order of Et-TIC << *i*Pr-TIC < *i*Pr-TACN < Me-TPM < Et-TPM < *i*Pr-TPM. For both the TIC and TPM ligands, the reactivity of the copper(I) nitrite complex increased with a decrease in the steric effect of the substituent of the ligand.

MO Calculation. To gain further insight into the electronic structure and reactivity of the copper(I) nitrite complex, molecular orbital (MO) calculations were carried out for copper(I) nitrite complexes with TIC, TPM, and TACN ligands. For comparison, MO calculations were also done for free copper(I) ion, TIC, TPM, and TACN ligands, and their copper(I) complexes. The substituents of TIC, TPM, and TACN ligands were replaced with hydrogen (H) to simplify the systems for calculations. The optimized structures and their selected bond parameters for copper(I) nitrite complexes with TIC, TPM, and TACN ligands are shown in Figure S10 and Table S4 of the Supporting Information. The coordination geometries of the optimized structures belong to C_{3v} in TACN and TPM and a slightly distorted C_{3v} in TIC. The Cu−N_L and Cu−$N_{nitrite}$ bond lengths for the optimized structures were shorter and longer than those obtained from the X-ray crystal structures, respectively. These structural changes may have resulted from loss of the steric effect of the substituent in the calculations. In spite of

Table 3. Summary of Selected Spectroscopic Data for Copper(II) Acetate Complexes

complex	UV–vis λ_{max}/nm (ϵ/ M^{-1} cm^{-1}) in CH_2Cl_2	EPR *g*-values, $A_{//}$ (mT) 4 K in CH_2Cl_2	ESI-MS *m/z* (relative intensity)
(*i*Pr-TIC)Cu(O_2CCH_3)$_2$	260 (4100), 697 (100)	$g_\perp = 2.07$, $g_{//} = 2.30$, $A_{//} = 15.2$	520 (100), [(*i*Pr-TIC)Cu(O_2CCH_3)]$^+$
(Et-TIC)Cu(O_2CCH_3)$_2$	261 (3800), 705 (100)	$g_\perp = 2.08$, $g_{//} = 2.30$, $A_{//} = 15.9$	478 (100), [(Et-TIC)Cu(O_2CCH_3)]$^+$
(*i*Pr-TPM)Cu(O_2CCH_3)$_2$	283 (3900), 390 (500), 706 (90)	$g_\perp = 2.07$, $g_{//} = 2.30$, $A_{//} = 16.1$	588 (100), [(*i*Pr-TPM)Cu(O_2CCH_3)]$^+$
(Et-TPM)Cu(O_2CCH_3)$_2$	271 (4100), 388 (590), 702 (80)	$g_\perp = 2.07$, $g_{//} = 2.30$, $A_{//} = 16.1$	504 (100), [(Et-TPM)Cu(O_2CCH_3)]$^+$
(Me-TPM)Cu(O_2CCH_3)$_2$	270 (3700), 390 (650), 699 (70)	$g_\perp = 2.07$, $g_{//} = 2.30$, $A_{//} = 15.8$	420 (100), [(Me-TPM)Cu(O_2CCH_3)]$^+$
(*i*Pr-TACN)Cu(O_2CCH_3)$_2$	298 (4900), 684 (110)[a]	$g_\perp = 2.06$, $g_{//} = 2.30$, $A_{//} = 15.4$[a]	

[a] Reference 28.

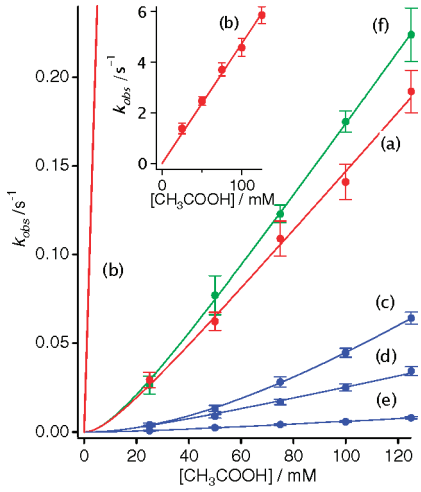

Figure 7. Plots of pseudo first-order rate constants, k_{obs}, against the concentration of acetic acid in CH_2Cl_2 at 293 K. (a) (*i*Pr-TIC)Cu(NO_2), (b) (Et-TIC)Cu(NO_2), (c) (Me-TPM)Cu(NO_2), (d) (Et-TPM)Cu(NO_2), (e) (*i*Pr-TPM)Cu(NO_2), and (f) (*i*Pr-TACN)Cu(NO_2). The solid lines show simulation curves fitted with eq 2.

Scheme 1

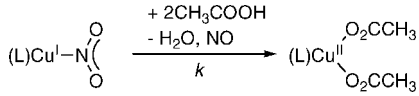

Scheme 2

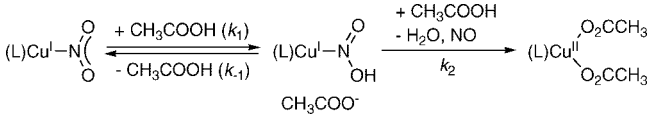

Table 4. Rate Constants for Reactions of Copper(I) Nitrite Complexes with Acetic Acid at 293 K

complex	k_1 (M^{-1} s^{-1})	k_{-1}/k_2 (M)
(*i*Pr-TIC)Cu(NO_2)	1.69 ± 0.11	0.0147 ± 0.0069
(Et-TIC)Cu(NO_2)	47.9 ± 1.0	~0
(*i*Pr-TPM)Cu(NO_2)	0.0821 ± 0.0045	0.0357 ± 0.0075
(Et-TPM)Cu(NO_2)	0.409 ± 0.014	0.0615 ± 0.055
(Me-TPM)Cu(NO_2)	1.22 ± 0.07	0.172 ± 0.016
(*i*Pr-TACN)Cu(NO_2)	2.08 ± 0.06	0.0195 ± 0.0030

the different bond lengths, the Cu−N_L and Cu−$N_{nitrite}$ bond lengths for the optimized structures increased in the order of TIC < TPM < TACN and TACN < TPM < TIC, which was the same order for the X-ray crystal measurements, respectively.

Orbital energies and their orbital character obtained from the MO calculations for free copper(I) ion, the TIC, TPM, and TACN ligands, and their copper(I) complexes and copper(I) nitrite complexes are summarized in Tables S5−S15 of the Supporting Information. Figure 8 shows the orbital diagram for

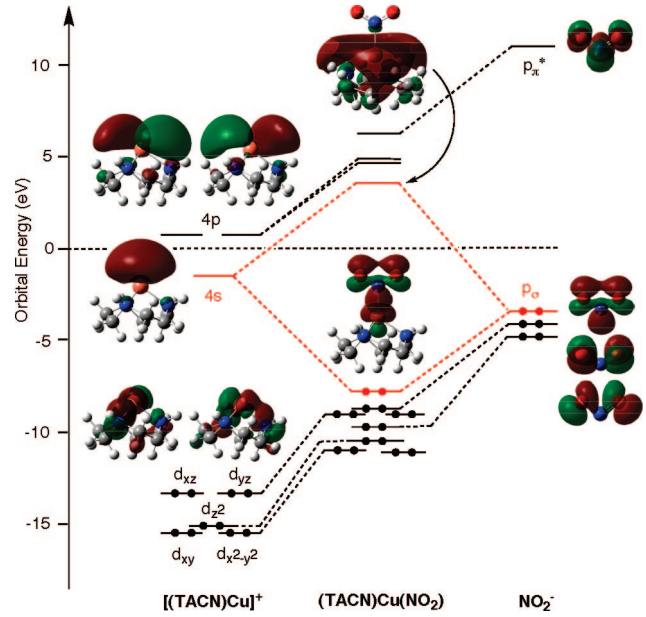

Figure 8. Orbital diagram for (TACN)Cu(NO_2).

(TACN)Cu(NO_2). The orbital energies for NO_2^-, [(TACA)Cu]$^+$, and (TACA)Cu(NO_2) were picked from Tables S9, S10, and S13 of the Supporting Information. As shown in Figure 8, the highest occupied molecular orbital (HOMO) for (TACN)Cu(NO_2) consists of an interaction between the unoccupied Cu(4s)-orbital of [(TACA)Cu]$^+$ and the occupied p_σ-orbital of NO_2^-. As a result, a part of the electron of NO_2^- transfers to the Cu side in (TACN)Cu(NO_2), and the N−O bond distance of the copper-bound NO_2^- becomes shorter than that of free NO_2^- (Figure 8 and Table S4 of the Supporting Information). As for (TACN)Cu(NO_2), the HOMOs for (TIC)Cu(NO_2) and (TPM)Cu(NO_2) comprised of interactions between the Cu(4s)-orbital and the p_σ-orbital, and, with coordination, the N−O bonds of the copper-bound NO_2^- became short.

To investigate electronic structural changes for the tridentate ligand, orbital energies for (TACN)Cu(NO_2), (TIC)Cu(NO_2), and (TPM)Cu(NO_2) were compared. As clearly seen in Figure 9, the orbital energies for the HOMOs and copper d-orbitals are changed by the tridentate ligand. Since the HOMO of the copper(I) nitrite complex interacts with the proton in the Cu-NiR reaction, the orbital energy for the HOMO would correlate to the Cu-NiR reactivity. The HOMO for (TIC)Cu(NO_2) is about 0.5 eV higher than those for (TACN)Cu(NO_2) and (TPM)-Cu(NO_2). To further investigate correlation of the energy of the HOMO and the Cu-NiR activity, the stabilization energy for protonation of the copper(I) nitrite complex was calculated using the Hartree–Fock method. The stabilization energies for protonation of (TACN)Cu(NO_2), (TIC)Cu(NO_2), and (TPM)-Cu(NO_2), with no solvent correction, were estimated to be 1133, 1173, and 1132 kJ/mol, respectively. The stabilization energy

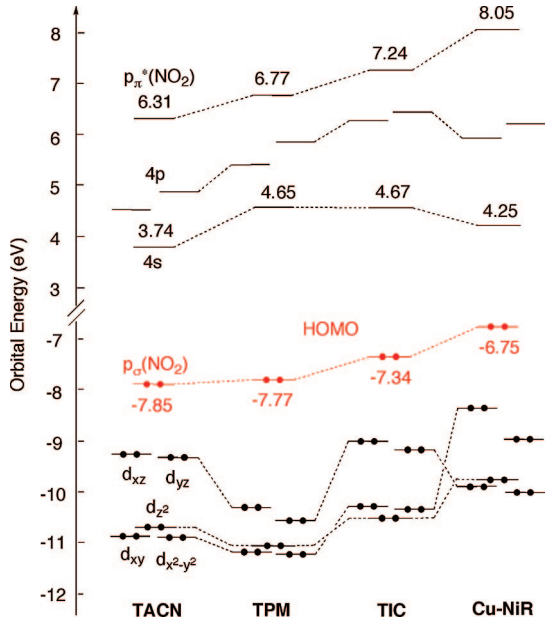

Figure 9. Comparison of energies of frontier molecular orbitals for copper(I) nitrite complexes. TACN, (TACN)Cu(NO_2); TPM, (TPM)-Cu(NO_2); TIC, (TIC)Cu(NO_2); and Cu-NiR, nitrite adduct to reduced type-2 Cu site.

for protonation of (TIC)Cu(NO_2) was about 40 kJ/mol larger than those of (TACN)Cu(NO_2) and (TPM)Cu(NO_2), and the value is close to the difference of the HOMOs (~0.5 eV: ~48 kJ/mol). All of these results suggest that the high Cu-NiR reactivity of the TIC complex results from the high energy of the HOMO.

To compare model complexes with Cu-NiR, the orbital energies for the nitrite adduct of the reduced type-2 Cu site were also calculated. The structural parameters and orbital energies are summarized in Tables S4, S16, and S17 of the Supporting Information. The $Cu-N_{Nitrite}$ bond length (2.095 Å) for the nitrite adduct of Cu-NiR was longer than that (2.001 Å) for (TIC)-Cu(NO_2). As for the model complexes, the HOMO for the nitrite adduct of Cu-NiR comprised of a bonding interaction between the unoccupied Cu(4s)-orbital and the occupied p_σ-orbital, and the N−O bonds of NO_2^- became short with coordination. The orbital energy for the HOMO of Cu-NiR was −6.75 eV, which is 0.59 eV higher than that of (TIC)Cu(NO_2). This suggests that the Cu-NiR reactivity of the nitrite adduct of Cu-NiR is higher than that of the model complexes.

Discussion

Effect of Tridentate Ligand on Cu-NiR Reactivity. This study reports structural and spectroscopic characterization of new copper(I) nitrite complexes of sterically hindered TIC and TPM ligands, which are close to the type-2 Cu site in Cu-NiR. The new characterization allows discussion of the effect of the tridentate ligand on Cu-NiR activity on the basis of structural and spectroscopic properties. All of the present copper(I) nitrite complexes have η^1-N coordination patterns of the copper-bound nitrites. However, their Cu-NiR activity was drastically changed by the electronic and steric effects of the tridentate ligand. The Cu-NiR activity increased in the order of *i*Pr-TPM < Et-TPM < Me-TPM < *i*Pr-TIC < *i*Pr-TACN << Et-TIC. Because the first protonation of the copper-bound nitrite is the rate-limiting step of the Cu-NiR reaction with acetic acid, this order would correlate to the electron density of the copper-bound nitrite and can be explained primarily by the electron donor effect of the tridentate ligand and second by the steric effect of the substituent.

With coordination to the copper, nitrite donates electrons from the occupied nitrite p_σ-orbital to the unoccupied Cu(4s)-orbital (σ-donation) and accepts electrons from the occupied Cu($3d_\pi$)-orbital to the unoccupied nitrite p_π*-orbital (π-back-donation). Since the σ-donation is more significant than the π-back-donation, the electron density of the copper-bound nitrite becomes smaller than that of the free nitrite ion. However, with an increase in the electron donor effect of the tridentate ligand, the electron density of the copper(I) ion increases, the σ-donation from the copper-bound nitrite decreases, and the π-back-donation from the copper increases. Therefore, the strong electron donor effect of the tridentate ligand operates to suppress the decrease in the electron density of the copper-bound nitrite. As a result, the Cu-NiR activity increases with an increase in the electron donor effect of the tridentate ligand. The electron donor effect of the tridentate ligand is controlled by the electron density of the N atom of the ligand and the $Cu-N_L$ bond length. The electron density of the N atom of the tridentate ligand would increase in the order of TPM < TIC < TACN, because it increases in the order of pyrazole < imidazole < amine.[37] This order is confirmed by the present MO calculations, in which the energy of the bonding N σ-orbital of the tridentate ligand increases in the order of TPM (−12.7 eV) < TIC (−11.6 eV) < TACN (−9.5 eV). In contrast, as shown in the X-ray crystal structures, the $Cu-N_L$ bond length increases in the order of TIC < TPM < TACN. Although TACN has the most electron-dense N atom of these three ligands, the fact that it also has the longest $Cu-N_L$ bond length weakens its electron donation to the copper ion. Conversely, TIC has a moderately electron-dense N atom but the shortest $Cu-N_L$ bond length, which strengthens the electron donation. Overall, the electron donor effect of the tridentate ligand increases in the order of TPM < TACN ≤ TIC. This order is supported by a recent report of the CO stretching frequencies (ν_{CO}) and ^{63}Cu NMR shifts of these copper(I) carbonyl complexes, which correlate with the electron density of the copper(I) ion, TPM < TACN ≤ TIC.[32]

This study clearly shows that the Cu-NiR activity increases with a decrease in the steric effect of the substituent: *i*Pr < Et < Me. The steric effect of the substituent controls the Cu-NiR activity with changes in the $Cu-N_{nitrite}$ bond length. With a decrease in the bulkiness of the substituent, the steric repulsion between the substituent and the copper-bound nitrite becomes smaller, resulting in a shorter $Cu-N_{nitrite}$ bond length. This is clearly seen in the present X-ray crystal structures; the $Cu-N_{nitrite}$ bond length becomes 0.141 Å shorter by going from *i*Pr-TIC to Et-TIC and 0.127 Å shorter by going from *i*Pr-TPM to Me-TPM. As the $Cu-N_{nitrite}$ bond length shortens, the π-back-donation from the occupied Cu($3d_\pi$)-orbital to the unoccupied nitrite p_π*-orbital is stronger, and the electron density of the copper-bound nitrite is larger. Moreover, the $Cu-N_{nitrite}$ bond becomes stronger as the $Cu-N_{nitrite}$ bond length becomes shorter. The strong $Cu-N_{nitrite}$ bond would suppress the dissociation of the copper-bound nitrite with its protonation and assist in an efficient Cu-NiR reaction. The increase in the π-back-donation can be manifested in the copper-nitrite stretching frequencies

(37) (a) Martell, A. E.; Smith, R. M. *Critical Stability Constants*; Plenum Press: New York; Vol. I–III. (b) Albert, A. In *Physical Methods in Heterocyclic Chemistry*; Katritzky, A. R., Ed.; Academic Press: New York, 1971; Vol. III, pp 1–108. (c) Yang, R.; Zompa, L. J. *Inorg. Chem.* **1976**, *15*, 1499–1502.

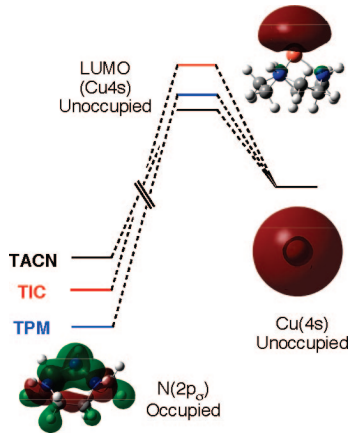

Figure 10. Interaction of occupied σ-orbital of the ligand and the LUMO, Cu(4s), of the copper(I) ion. The pictures of MOs are taken for TACN.

(ν_{Cu-N}) for the TPM complexes: *i*Pr < Et < Me. For the TIC complexes, the steric effect of the substituent also affects the Cu−N_L bond length. As shown in the X-ray crystal structure, the average (2.063 Å) of three Cu−N_L bond lengths for Et-TIC is much shorter than that (2.139 Å) for *i*Pr-TIC. Therefore, the steric effect of the substituent in TIC controls not only the π-back-donation with the Cu−$N_{nitrite}$ bond length but also the electron density of the copper ion with the Cu−N_L bond length. This may result in a drastic increase in the Cu-NiR activity by going from *i*Pr-TIC to Et-TIC. In addition, the significant steric effect of *i*Pr-TIC, manifested in its X-ray crystal structure, may reverse its order relative to *i*Pr-TACN.

The present MO calculations for copper(I) nitrite complexes corroborate the above discussion and also afford additional insight into the effect of the tridetate ligand on Cu-NiR activity. The Cu-NiR activity correlates with the energy of the HOMO of the copper(I) nitrite complex, because the HOMO is the molecular orbital that interacts with protons. With an increase in the energy of the HOMO, the protonation of the copper-bound nitrite becomes faster, leading to higher Cu-NiR activity. As shown in Figure 8, since the HOMO of the copper(I) nitrite complex is comprised of the bonding interaction between the unoccupied Cu(4s)-orbital of $[(L)Cu]^+$ and the occupied p_σ-orbital of NO_2^-, the energy of the HOMO is determined by that of the unoccupied Cu(4s)-orbital of $[(L)Cu]^+$. As shown in Figure 10, the energy of the Cu(4s)-orbital of $[(L)Cu]^+$ increases in the order of TACN < TPM < TIC, although that of the bonding N σ-orbitals of the tridentate ligand increases in the order of TPM < TIC < TACN. The imino-type ligand binds to a copper ion via the σ- and π-orbitals of the imino N atom, while the amino-type ligand binds with the σ-orbital of the amino N atom. Furthermore, the imino-type ligand can accept electrons by a π-back-donation from a copper ion in the π^*-orbital of the ligand. The electronic nature of the imidazole ligand, that is, the combination of the relatively high energy of the bonding N σ-orbital and the strong interaction with the copper(I) ion, gives TIC the high Cu-NiR activity. Finally, the O atom of the copper-bound nitrite will protonate, because the MO calculations show large electron densities on the O atoms of the nitrite in the HOMO.

Biological Relevance. Our discussion has focused on the structure of the nitrite adduct for reduced Cu-NiR and the role of the highly conserved $(His)_3$ environment of the type-2 copper site in the Cu-NiR reaction. Many reports have outlined the structures of copper(II) nitrite complexes.[15–25] Most copper(II) nitrite complexes contain an O-bound nitrito moiety, based on either η^1-O, η^2-O,O, or η^2-O,O′ coordination. In fact, recent X-ray crystal structural studies of oxidized Cu-NiR soaked nitrite have shown asymmetric bidentate O-nitrito coordination, η^2-O,O′, with the copper(II) ion in the oxidized type-2 Cu site.[8b,c,9c] By contrast, as shown in previous[27,28] and present studies, all copper(I) nitrite complexes have the η^1-N coordination pattern. The η^1-N coordination pattern is preferable to O-nitrite coordination for the binding of the nitrite to the copper(I) ion. Although further studies on the steric and electronic effects of the amino acid residues around the type-2 Cu site on the coordination structure of nitrite are required, these results suggest that the coordination structure of the copper-bound nitrite may change from O-nitrito coordination to η^1-N coordination with reduction of the type-2 Cu site.

The $(His)_3$ coordination environment of the type-2 Cu site in Cu-NiR is highly conserved in all Cu-NiR. However, in previous studies, the role of the $(His)_3$ coordination environment in the Cu-NiR reaction has not been discussed. The present results suggest that the $(His)_3$ coordination environment of the type-2 Cu site would play an essential role in the increase of the Cu-NiR activity because the $(His)_3$ coordination environment is similar to that of the TIC complex. As shown in Table 1, the average Cu−N_L bond length (2.00 Å) of Cu-NiR is shorter than that (2.063 Å) of (Et-TIC)Cu(NO_2), suggesting that the electron donor effect of the $(His)_3$ ligands of the type-2 Cu site is much stronger than that of Et-TIC. In fact, this is supported by the results showing that the CO stretching frequency (ν_{CO} = 2050 cm^{-1}) for the CO adduct of the type-2 Cu site is much lower than that (ν_{CO} = 2076 cm^{-1}) of Et-TIC.[32,38] Furthermore, the steric effect of the $(His)_3$ ligand in Cu-NiR is much smaller than that of Et-TIC because there is no substituent in the imidazolyl moiety of histidine. The stronger donor effect and the lesser steric effect of the type-2 Cu site suggest much higher Cu-NiR activity than Et-TIC. This is supported by the present MO calculations, in which the energy of the HOMO for the Cu-NiR is much higher than that for the model complexes (see Figure 9).

Experimental Section

General Considerations. All metal complexes were prepared and stored in a glovebox under Ar atmosphere. Anhydrous solvents were purchased from commercial sources and degassed before use. (*i*Pr-TACN)Cu(NO_2),[28] [(*i*Pr-TIC)Cu(CH_3CN)]ClO_4,[31] [(Et-TIC)-Cu(CH_3CN)]ClO_4,[31] [(*i*Pr-TPM)Cu(CH_3CN)]ClO_4,[32] [(Me-TPM)-Cu(CH_3CN)]ClO_4,[32] (OEP)Fe (OEP = octaethylporphyrinate),[39] and (OEP)Fe(NO)[39] were synthesized as described in the literature. All other reagents were obtained from commercial sources and used as received. ^{1}H NMR (500 MHz) and ^{15}N NMR (50.55 MHz) spectra were recorded on a JEOL JNM-LA500 spectrometer. ^{1}H NMR and ^{13}C NMR chemical shifts were reported versus tetramethylsilane and referenced to residual solvent peaks. ^{15}N NMR spectra were referenced to external $Na^{15}NO_3$ in D_2O. Fourier transform infrared (FT-IR) spectra were recorded on a JASCO FT/IR-460 spectrometer as KBr pellets. Far-FT-IR spectra were recorded on a JASCO FT/IR-6100 spectrometer as CsI pellets. UV–vis spectra were recorded on an Agilent 8453 spectrophoto-

(38) (a) Zhang, H.; Boulanger, M. J.; Mauk, A. G.; Murphy, M. E. P. *J. Phys. Chem. B* **2000**, *104*, 10738–10742. (b) Averill, B. A.; Wang, Y.; Ka, J. O.; Roublevskaia, I. N.; Tiedje, J. M. In *Biological Electron Transfer Chains: Genetics, Composition and Mode of Operation*; Vijgenboom, G. W. C. E., Ed.; Kluwer Academic Publications: Dordecht, The Netherlands, 1998; pp 185–196.
(39) Scheidt, W. R.; Duval, H. F.; Neal, T. J.; Ellison, M. K. *J. Am. Chem. Soc.* **2000**, *122*, 4651–4659.

Table 5. Crystallographic Data for Copper(I) Nitrite Complexes

	(*i*Pr-TIC)Cu(NO_2)	(Et-TIC)Cu(NO_2)-acetone	(*i*Pr-TPM)Cu(NO_2)	(Et-TPM)Cu(NO_2)	(Me-TPM)Cu(NO_2)
empirical formula	$C_{22}H_{34}N_7O_3Cu$	$C_{22}H_{34}N_7O_4Cu$	$C_{28}H_{46}N_7O_2Cu$	$C_{22}H_{34}N_7O_2Cu$	$C_{16}H_{22}N_7O_2Cu$
crystal system	monoclinic	monoclinic	monoclinic	monoclinic	orthorhombic
mol wt	508.10	524.10	576.26	492.10	407.94
space group	$P2_1$	$P2_1/c$	$P2_1/n$	Pa	$Pnma$
a/Å	8.817 (3)	9.824 (4)	9.901 (2)	9.409 (3)	18.196 (3)
b/Å	16.056 (5)	16.355 (5)	16.451 (2)	13.841 (4)	13.135 (2)
c/Å	9.010 (3)	14.914 (6)	20.166 (3)	9.811 (3)	7.773 (1)
β/deg	108.558 (7)	90.970 (1)	109.61 (3)	113.179 (6)	
V/Å^3	1209.1 (7)	2396.17 (8)	3094.3 (8)	1174.54 (6)	1857 (1)
Z	2	4	4	2	4
D_{calcd}/g cm^{-3}	1.395	1.453	1.237	1.391	1.458
μ(Mo Kα)/cm^{-1}	9.41	9.55	7.41	9.63	12.02
$2\theta_{max}$/deg	54.9	55.0	55.0	55.0	55.0
no of reflections	2810	5718	7039	2655	2182
no of variables	299	307	374	289	136
$R1$ ($I > 2\sigma(I)$)	0.074	0.076	0.071	0.080	0.069
$wR2$	0.206	0.205	0.171	0.212	0.168

meter (Agilent Technologies). Electrochemical experiments were performed using an ALS612A electrochemical analyzer (BAS). EPR spectra were recorded at room temperature on an E500 continuous-wave X-band spectrometer (Bruker). For EPR measurements at 4 K, an ESR910 helium-flow cryostat (Oxford Instruments) was used. Electrospray ionization (ESI) mass spectra were obtained with a LCT time-of-flight mass spectrometer equipped with an electrospray ionization interface (Micromass). Elemental analyses were performed at the Research Center for Molecular-Scale Nanoscience, Institute for Molecular Science. Stopped-flow kinetic measurements were performed with a UNISOKU stopped-flow instrument equipped with a LAUDA RE104 thermostat.

Safety Note. Caution! Perchlorate salts are potentially explosive, and only a small amount of material should be used, and it should be handled with great care.

Preparation of Et-TPM. Et-TPM was synthesized by the same procedure used for Me-TPM:[40] 3,5-diethylpyrazole as a starting material in 67% yield. ^{1}H NMR ($CDCl_3$): δ 8.08 (1H, s), 5.91 (3H, s), 2.54 (6H, q, J = 7.7 Hz), 2.36 (6H, q, J = 7.5 Hz), 1.15 (9H, t, J = 7.7 Hz), 1.06 (9H, t, J = 7.5 Hz). ^{13}C NMR ($CDCl_3$): δ 154.1, 147.0, 103.7, 80.5, 21.6, 18.4, 13.6, 12.3. IR (KBr, cm^{-1}): 2970, 2938, 2878, 1558, 1457, 1374, 1309, 1264, 1052, 1008, 956, 881, 855, 838, 808. ESI-MS (CH_3OH): 383.29 (Et-TPM + H^+).

Preparation of [Et-TPMCu(CH_3CN)]ClO_4. To a solution of Et-TPM (571 mg, 1.49 mmol) in THF (10 mL), solid [Cu(CH_3CN)$_4$]ClO_4 (488 mg, 1.49 mmol) was added. The resulting mixture was stirred for 2 h at ambient temperature and then filtered. After addition of pentane (10 mL) to the filtrate with rapid stirring, a colorless precipitate was filtered. Recrystallization from CH_3CN/Et_2O gave the product as colorless crystals (632 mg, 1.08 mmol, 72% yield). ^{1}H NMR (CD_2Cl_2): δ 7.76 (1H, s), 6.02 (3H, s), 2.79 (6H, q, J = 7.4 Hz), 2.66 (6H, q, J = 7.6 Hz), 2.16 (3H, s), 1.36 (9H, t, J = 7.4 Hz), 1.22 (9H, t, J = 7.7 Hz). IR (KBr, cm^{-1}): 2972, 2939, 2880, 1559, 1456, 1425, 1400, 1379, 1297, 1256, 1236, 1145, 1115, 1078, 1017, 989, 965, 897, 843, 821, 795, 711, 677, 625. Anal. Calcd for $C_{25}H_{38.5}N_{7.5}ClCuO_4$ [TPM^{Et}Cu(CH_3CN)]ClO_4·0.5CH_3CN: C, 49.46; H, 6.39; N, 17.30. Found: C, 49.43; H, 6.34; N, 17.14.

Preparation of (*i*Pr-TIC)Cu(NO_2). To a solution of [(*i*Pr-TIC)Cu(CH_3CN)]ClO_4 (271 mg, 0.450 mmol) in CH_2Cl_2 (5 mL) was added an acetone solution (3 mL) of [(Ph_3P)$_2$N]NO_2 (263 mg, 0.450 mmol). After the resultant mixture was stirred for 1 h at ambient temperature, the yellow precipitate was filtered off. Recrystallization from MeOH/Et_2O gave the product as yellow crystals (136 mg, 0.268 mmol, 60% yield). ^{1}H NMR (CD_2Cl_2): δ 7.01 (3H, s), 4.81 (1H, br), 3.63 (9H, s), 3.21 (3H, septet, J = 7.0 Hz), 1.50 (18H, d, J = 6.8 Hz). IR (KBr, cm^{-1}): 2962, 2925, 2871, 1576, 1473, 1415, 1384, 1320 (1296 $^{15}NO_2^-$), 1260 (1235 $^{15}NO_2^-$), 1182, 1124, 1090, 902, 875, 831 (824 $^{15}NO_2^-$), 766, 747, 728, 670. Anal. Calcd for $C_{22}H_{34}N_7CuO_3$: C, 52.01; H, 6.75; N, 19.30. Found: C, 51.73; H, 6.67; N, 19.14.

Preparation of (Et-TIC)Cu(NO_2). To a solution of [(Et-TIC)Cu(CH_3CN)]ClO_4 (205 mg, 0.366 mmol) in CH_2Cl_2 (5 mL) was added an acetone solution (5 mL) of [(Ph_3P)$_2$N]NO_2 (214 mg, 0.366 mmol) at −20 °C. After the resultant mixture was stirred for 1 h at −20 °C, the solution was evaporated. The residue was washed with acetone (5 mL), followed by recrystallization from CH_2Cl_2/acetone at −20 °C. The product was obtained as yellow crystals (112 mg, 0.240 mmol, 66% yield). ^{1}H NMR (CD_2Cl_2): δ 7.01 (3H, s), 4.95 (1H, br), 3.62 (9H, s), 2.79 (6H, q, J = 7.5 Hz), 1.31 (9H, t, J = 7.2 Hz). IR (KBr, cm^{-1}): 2974, 2937, 2874, 1574, 1485, 1455, 1415, 1376, 1271 (1244 $^{15}NO_2^-$), 1206, 1176, 1134, 1072, 993, 889, 769, 732. Anal. Calcd for $C_{20.5}H_{31}N_7CuO_{3.5}$ [(Et-TIC)Cu(NO_2)·0.5acetone]: C, 49.74; H, 6.31; N, 19.81. Found: C, 49.53; H, 6.39; N, 19.58.

Preparation of (*i*Pr-TPM)Cu(NO_2). To a solution of [(*i*Pr-TPM)Cu(CH_3CN)]ClO_4 (257 mg, 0.383 mmol) in acetone (5 mL) was added an acetone solution (3 mL) of [(Ph_3P)$_2$N]NO_2 (224 mg, 0.383 mmol). After the resultant solution was stirred for 1 h at ambient temperature, Et_2O (10 mL) was added to the solution with stirring. The pale-yellow powder was filtered off and then crystallized from CH_2Cl_2/Et_2O to afford the product as yellow crystals (105 mg, 0.182 mmol, 48% yield). ^{1}H NMR ($CDCl_3$): δ 7.86 (1H, s), 5.92 (3H, s), 3.42 (3H, septet, J = 8.6 Hz), 3.00 (3H, septet, J = 8.6 Hz), 1.27 (18H, d, J = 8.6 Hz), 1.21 (18H, d, J = 8.5 Hz). IR (KBr, cm^{-1}): 2966, 2930, 2868, 1555, 1468, 1401, 1382, 1363, 1311 (1289 $^{15}NO_2^-$), 1282 (1263 $^{15}NO_2^-$), 1233, 1181, 1104, 1056, 1008, 915, 880, 823, 814 (808 $^{15}NO_2^-$), 799, 724, 669. Anal. Calcd for $C_{28}H_{46}N_7CuO_2$: C, 58.36; H, 8.05; N, 17.01. Found: C, 58.08; H, 8.09; N, 16.88.

Preparation of (Et-TPM)Cu(NO_2). To a solution of (Et-TPM)Cu(CH_3CN)ClO_4 (213 mg, 0.363 mmol) in acetone (5 mL) was added an acetone solution (3 mL) of [(Ph_3P)$_2$N]NO_2 (213 mg, 0.364 mmol). After the resultant solution was stirred for 1 h at ambient temperature, the pale-yellow powder was filtered off. Crystallization from CH_2Cl_2/Et_2O afforded the product as yellow crystals (114 mg, 0.232 mmol, 64% yield). ^{1}H NMR ($CDCl_3$): δ 7.81 (1H, s), 6.10 (3H, s), 2.91 (6H, q, J = 7.6 Hz), 2.85 (6H, q, J = 7.3 Hz), 1.46 (9H, t, J = 7.3 Hz), 1.30 (9H, t, J = 7.7 Hz). IR (KBr, cm^{-1}): 2976, 2939, 2880, 1559, 1464, 1401, 1379, 1311, 1283 (1261 $^{15}NO_2^-$), 1235, 1161, 1051, 1016, 990, 964, 897, 842, 813 (806 $^{15}NO_2^-$), 709, 630. Anal. Calcd for $C_{22}H_{34}N_7CuO_2$: C, 53.70; H, 6.96; N, 19.92. Found: C, 53.43; H, 6.95; N, 19.77.

Preparation of (Me-TPM)Cu(NO_2). To a solution of (Me-TPM)Cu(CH_3CN)ClO_4 (239 mg, 0.476 mmol) in CH_2Cl_2 (5 mL) was added an acetone solution (3 mL) of [(Ph_3P)$_2$N]NO_2 (278 mg,

(40) Juliá, S.; del Mazo, J.; Avila, L. *Org. Prep. Proc. Int.* **1984**, *16*, 299–307.

0.476 mmol). After the resultant mixture was stirred for 1 h at ambient temperature, the yellow precipitate was filtered off, washed with acetone (5 mL), and dried under vacuum (158 mg, 0.387 mmol, 81% yield). For X-ray analysis, yellow crystals of the product were obtained from CH_2Cl_2 at −20 °C. ^{1}H NMR (CD_2Cl_2): δ 7.73 (1H, s), 6.03 (3H, s), 2.55 (9H, s), 2.47 (9H, s). IR (KBr, cm^{-1}): 3141, 2985, 2957, 2922, 1567, 1465, 1415, 1390, 1314 (1289 $^{15}NO_2^-$), 1280 (1258 $^{15}NO_2^-$), 1240, 1154, 1099, 1039, 980, 898, 849, 822 (814 $^{15}NO_2^-$), 801, 705, 698, 630. Anal. Calcd for $C_{16}H_{22}N_7CuO_2$: C, 47.11; H, 5.44; N, 24.03. Found: C, 46.83; H, 5.41; N, 24.17.

Preparation of (*i*Pr-TIC)Cu(O_2CCH_3)$_2$. To a solution of (*i*Pr-TIC) (137 mg, 0.344 mmol) in CH_2Cl_2 (5 mL) was added $Cu(O_2CCH_3)_2 \cdot H_2O$ (69 mg, 0.35 mmol) as a solid. The resultant mixture was stirred for 1 h at ambient temperature and then filtered to remove any remaining solid. The filtrate was evaporated followed by recrystallization from CH_2Cl_2−Et_2O, causing the precipitation of the product as a green crystalline solid (137 mg, 0.236 mmol, 69% yield). IR (KBr, cm^{-1}): 2969, 2935, 2878, 1561, 1523, 1478, 1407, 1137, 1091, 1007, 949, 906, 879, 785, 693, 618. Anal. Calcd for $C_{26}H_{44}N_6CuO_7$ [(iPr-TIC)Cu(O_2CCH_3)$_2 \cdot 2H_2O$]: C, 50.68; H, 7.20; N, 13.64. Found: C, 50.97; H, 7.14; N, 13.35.

Preparation of (Et-TIC)Cu(O_2CCH_3)$_2$. The complex was prepared in 61% yield by the same method with (*i*Pr-TIC)-Cu(O_2CCH_3)$_2$ as described above. IR (KBr, cm^{-1}): 2969, 2935, 2876, 1579, 1485, 1414, 1338, 1202, 1177, 1149, 1073, 1030, 899, 784, 772, 763, 695, 683, 671, 634, 509. Anal. Calcd for $C_{23}H_{36}N_6CuO_6$ [(Et-TIC)Cu(O_2CCH_3)$_2 \cdot H_2O$]: C, 49.67; H, 6.53; N, 15.11. Found: C, 49.48; H, 6.62; N, 15.02.

Reaction of Copper(I) Nitrite Complex with Acetic Acid. To a solution of copper(I) nitrite complex (0.15 mmol) in CH_2Cl_2 (3 mL) was added a CH_2Cl_2 solution (1 mL) of acetic acid (18 μL, 0.31 mmol), causing the solution to become either green or blue. Removal of solvent followed by crystallization from CH_2Cl_2/Et_2O yielded a crystalline product. The product was identified as $TIC^RCu(O_2CCH_3)_2$ by comparison of UV–vis, IR, and EPR spectra to those of independently synthesized material. R = *i*Pr: 58 mg, 0.10 mmol, 67% yield. R = Et: 60 mg, 0.11 mmol, 73% yield.

Reaction of R-TPMCu(NO_2) (R = *i*Pr, Et, and Me) with CH_3COOH. To a solution of $TPM^RCu(NO_2)$ (0.15 mmol) in CH_2Cl_2 (3 mL) was added a CH_2Cl_2 solution (1 mL) of CH_3COOH (18 μL, 0.31 mmol), causing the solution to become blue. Removal of solvent followed by crystallization from CH_2Cl_2/Et_2O yielded a blue crystalline solid. The product was identified as $Cu(O_2CCH_3)_2 \cdot H_2O$ from IR spectrum and elemental analysis in each case of (iPr-TPM), (Et-TPM), and (Me-TPM).

Detection of NO Generated from (L)Cu(NO_2). A solution of (L)Cu(NO_2) in CH_2Cl_2 (0.50 mM, 1.0 mL) was prepared in a small vial. The vial was placed in a larger vial containing a solution of (OEP)Fe in CH_2Cl_2 (0.50 mM, 1.0 mL) and then capped with a rubber septum. A solution of acetic acid or trifluoroacetic acid in CH_2Cl_2 (50 mM, 20 μL) was added to the solution of (L)Cu(NO_2) with a syringe, and then the vial was kept at room temperature for 12 h. EPR measurement of the (OEP)Fe solution at room temperature showed an EPR signal typical for (OEP)Fe(NO) (g = 2.05, A = 1.53 mT). Yields of (OEP)Fe(NO) were estimated by comparing the intensities of the EPR signals (Figure S4 of the Supporting Information) to that of the authentic (OEP)Fe(NO) sample (L = (*i*Pr-TIC), 56%; L = (*i*Pr-TPM), 26%; L = TIC^{Me}, 32%; and L = (iPr-TACN), 17%).

Kinetics. Kinetic studies of nitrite reduction of (L)Cu(NO_2) were carried out by monitoring the changes of the UV–vis spectra at 20 °C. For (Et-TIC)Cu(NO_2), (*i*Pr-TIC)Cu(NO_2), and (*i*Pr-TACN)-Cu(NO_2), the reaction was started by the mixing of a solution of (Et-TIC)Cu(NO_2), (*i*Pr-TIC)Cu(NO_2), or (*i*Pr-TACN)Cu(NO_2) in CH_2Cl_2 (0.50 mM) and a solution of CH_3COOH in CH_2Cl_2 (50, 100, 150, 200, and 250 mM) with a stopped-flow instrument. For R-TPMCu(NO_2) (R = *i*Pr, Et, or Me), the reaction was initiated by the addition of CH_3COOH (5.7, 11.4, 17.2, 22.9, and 28.6 μL) to a solution of R-TPMCu(NO_2) in CH_2Cl_2 (0.25 mM) in a quartz cell capped with a rubber septum.

X-ray Data Collection. Diffraction measurements for the single crystals of (*i*Pr-TIC)Cu(NO_2), (Et-TIC)Cu(NO_2), (*i*Pr-TPM)-Cu(NO_2), (Et-TPM)Cu(NO_2), and (Me-TPM)Cu(NO_2) were made with Mo Kα radiation (λ = 0.71070 Å) on a Rigaku MSC Mercury charge-coupled device (CCD) at 173 K. The data were corrected for Lorentz polarization effects. Empirical absorption corrections were applied. The structures were solved by a combination of a direct method (SIR92)[41] and Fourier synthesis (DIRDIF94).[42] The structures were refined by a full-matrix least-squares method using the TEXSAN crystallographic software package (Molecular Structure Corporation). Non-hydrogen atoms were refined anisotropically. Hydrogen atoms were placed at calculated positions except for the O−H moieties in (*i*Pr-TIC)Cu(NO_2) and (Et-TIC)Cu(NO_2) and refined isotropically. Crystallographic data and the results of refinements are summarized in Table 5. During the refinement of (*i*Pr-TPM)Cu(NO_2), O atoms in the copper-bound nitrite were found to be disordered and refined by taking into account two components (O1,O2:O3,O4 = 0.48:0.52).

Quantum-Chemical Calculations. The quantum-chemical calculations were performed using the Gaussian03 program package.[43] A modified Wachters' basis set (14s13p5d)/[9s9p3d] was used for Cu, 6-31G(d) for N close to Cu, and 6-31G for the other atoms.[44] GaussView03 was used for drawing orbital pictures.[45] The optimized structures of copper(I) nitrite complexes were calculated using B3LYP density functional methods. Calculations of molecular orbital energies and coefficients and total energies were carried out using the Hartree–Fock method. Coordinates of a reduced type-2 Cu site of NiR were taken from the protein data bank file 1AQ8. To simplify the calculation for the nitrite adduct of the type-2 Cu site, three different Cu−N_L bond lengths were fixed at 2.00 Å, which affords a minimum of energy for the reduced type-2 Cu site and almost the average of the three Cu−N_L bond lengths.

Acknowledgment. This work was supported by grants from the Ministry of Education, Culture, Sports, Science and Technology, Japan, and from the Japan Science and Technology Agency, CREST.

Supporting Information Available: Text (PDF) containing additional figures (Figures S1−S10), tables (Tables S1−S17), and complete ref 43. X-ray crystallographic data (CIF). This material is available free of charge via the Internet at http://pubs.acs.org.

JA075575B

(41) Altomare, A.; Cascarano, G.; Giacovazzo, C.; Guagliardi, A.; Burla, M. C.; Polidoli, G.; Camalli, M. *J. Appl. Crystallogr.* **1994**, *27*, 435.
(42) Beurskens, P. T.; Admiraal, G.; Beurskens, G.; Bosman, W. P.; de Gelder, R.; Israel, R.; Smits, J. M. M. *The DIRDIF-94 Program System*; Technical Report for the Crystallography Laboratory; University of Nijmegen: Nijmegen, The Netherlands, 1994.
(43) Frisch, M. J. Gaussian03, revision C.03; Gaussian, Inc.: Wallingford, CT, 2004.
(44) Wachters, A. J. H. *J. Chem. Phys.* **1970**, *52*, 1033.
(45) Dennington, R., II; Keith, T.; Millam, J.; Eppinnett, K.; Hovell, W. L.; Gilliland, R. Semichem, Inc., Shawnee Mission, KS, 2003.